Key Engineering Materials Vols. 145-149 (1998) pp. 77-82
online at http://www.scientific.net

Analysis of Newly Defined Stress Intensity Factors at the End of Rectangular and Cylindrical Inclusions

N.-A. Noda[1], Q. Wang[2], T. Morodomi[1] and Y. Uemura[1]

[1] Department of Mechanical Engineering, Kyushu Institute of Technology
Kitakyushu 804, Japan

[2] Department of Material Engineering, Shandong University of Technology,
Jinan 250061, China

Keywords: Elasticity, Composite Material, Body Force Method, Rectangular Inclusions, Cylindrical Inclusions, Fiber, End Effect, Stress Intensity Factor, Singular Integral Equation

ABSTRACT

In short fiber reinforced composite it is known that the singular stress at the end of fibers causes crack initiation and final failure. This paper deals with this end effect in analyzing models of fiber as 2D rectangular and 3D cylindrical inclusions. The body force method is used to formulate the problems as a system of singular integral equations having Cauchy and logarithmic singularities. Initially, numerical solution of the singular integral equations is discussed. Next, interaction of rectangular inclusions are considered. Finally, singular stress at the end of a cylindrical inclusion is analyzed and discussed in comparison with the results of a rectangular inclusion.

1. INTRODUCTION

In this paper magnitudes of singular stress field at the end of reinforced fibers in composite materials are analyzed. In short fiber reinforced composites it is known that the singular stress at the end of fibers causes crack initiation and final failure. Recently, Chen and Nisitani [1] have indicated that at the corners of inclusions there appear to be two types of stress singularities corresponding to mode I and mode II types of deformations. Then, they have calculated newly defined stress intensity factors at the end of a rectangular inclusion under various conditions [2, 3].

In this study, initially, the body force method is used to formulate the problems as a system of singular integral equations having Cauchy and logarithmic singularities. Then, the numerical solution of the integral equations is discussed. Next, two equally shaped rectangular inclusions are assumed as a fundamental model, and the interaction of these inclusions are analyzed. Finally, singular stress at the end of a 3D cylindrical inclusion is analyzed considering actual fibers have 3D shapes in matrix. Then, the results are compared with the ones of a 2D rectangular inclusion.

2. THEORY AND SOLUTION

As a 3D model of a reinforced fiber in matrix a cylindrical inclusion is assumed in an infinite body (see Fig.1). The present method of analysis will be explained using the model of Fig.1. Here, L and D are sizes of the inclusion, and σ_z^∞ is a stress at infinity. The notations G_M, ν_M denote the shear modulus and Poisson's ratios of the matrix, respectively, and G_I, ν_I denote the ones of the inclusion. The problem is reduced to solving a system of singular integral equations (1) and (2), where the unknowns are body force densities distributed in an infinite body ' M ' that has the same elastic constants as those of the matrix, and in an infinite body ' I ' that has the same elastic constants as those of the inclusion [4].

$$-\frac{1}{2}F_{nM}(s)-\frac{1}{2}F_{nI}(s)+\int_L h_{nn}^{F_t M}(r_A,s)F_{tM}(r_A)dr_A+\int_L h_{nn}^{F_n M}(r_A,s)F_{nM}(r_A)dr_A$$

$$-\int_L h_{nn}^{F_{tI}}(r_A,s)F_{tI}(r_A)dr_A - \int_L h_{nn}^{F_{nI}}(r_A,s)F_{nI}(r_A)dr_A = -\sigma_{nM}^{\infty}(s) + \sigma_{nI}^{\infty}(s)$$

$$-\frac{1}{2}F_{tM}(s) - \frac{1}{2}F_{tI}(s) + \int_L h_{nt}^{F_tM}(r_A,s)F_{tM}(r_A)dr_A + \int_L h_{nt}^{F_nM}(r_A,s)F_{nM}(r_A)dr_A$$

$$-\int_L h_{nt}^{F_{tI}}(r_A,s)F_{tI}(r_A)dr_A - \int_L h_{nt}^{F_{nI}}(r_A,s)F_{nI}(r_A)dr_A = 0 \quad (1)$$

$$\int_L h_u^{F_tM}(r_A,s)F_{tM}(r_A)dr_A + \int_L h_u^{F_nM}(r_A,s)F_{nM}(r_A)dr_A - \int_L h_u^{F_{tI}}(r_A,s)F_{tI}(r_A)dr_A$$

$$-\int_L h_u^{F_{nI}}(r_A,s)F_{nI}(r_A)dr_A = -u_M^{\infty} + u_I^{\infty}$$

$$\int_L h_v^{F_tM}(r_A,s)F_{tM}(r_A)dr_A + \int_L h_v^{F_nM}(r_A,s)F_{nM}(r_A)dr_A - \int_L h_v^{F_{tI}}(r_A,s)F_{tI}(r_A)dr_A$$

$$-\int_L h_v^{F_{nI}}(r_A,s)F_{nI}(r_A)dr_A = -v_M^{\infty} + v_I^{\infty} \quad (2)$$

Here, F_{nM}, F_{tM}, F_{nI}, F_{tI} are the body force densities in the normal and tangential directions distributed in infinite bodies 'M' and 'I'. The notation $\int_L$ means integrating the body forces on the cylindrical boundary, $\sigma_{nM}^{\infty}(s)$ denotes normal stress appears at the point s in body M, and $h_{nn}^{F_{nM}}(r_A,s)$ denotes the normal stress induced at an collocation point when the body force with unit density in the normal direction is acting at the point r_A on the prospective boundary. Equations (1) and (2) enforce the boundary conditions along the interface $\sigma_{nM} - \sigma_{nI} = 0$, $\tau_{ntM} - \tau_{ntI} = 0$, $U_M - U_I = 0$ and $V_M - V_I = 0$, where (U_M, V_M) and (U_I, V_I) denote the displacements on the prospective boundary in infinite bodies 'M' and 'I', respectively, and $(\sigma_{nM}, \tau_{ntM})$ and $(\sigma_{nI}, \tau_{ntI})$ are tractions on the prospective boundary in infinite bodies 'M' and 'I', respectively.

In order to analyze eqn (1) and (2) accurately, the following method will be applied. The singular stress fields near the corner A can be expressed by two types of body force distributions in the normal and tangential directions, in other words, symmetric (mode I) and skew-symmetric (mode II) types distributions to the bisector of the corners [2,3]. In the vicinity of the corner A plain strain condition can be assumed and the character of the singular stress fields is determined from the eigenequations for two dimensional problems [1]. To approximate the unknown body force densities, they are approximated by a linear combination of weight functions and two fundamental density functions, that is, $r_A^{\lambda_1-1}$ and $r_A^{\lambda_2-1}$. Here r_A is a distance from the corner end A.

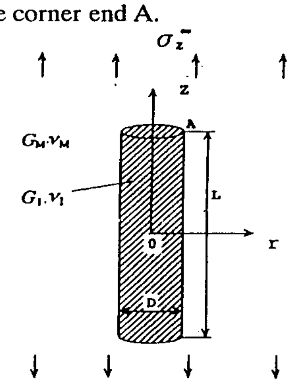

Fig.1 Cylindrical inclusion in an infinite body

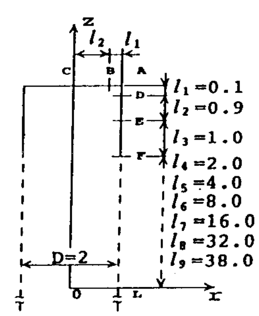

Fig.2 Boundary division for eqn(3), (4) when L/D=10^2

$$\begin{aligned} F_{tM}(r_A) &= F_{tM}^{\mathrm{I}}(r_A) + F_{tM}^{\mathrm{II}}(r_A) = W_{tM}^{\mathrm{I}}(r_A) r_A^{\lambda_1 - 1} + W_{tM}^{\mathrm{II}}(r_A) r_A^{\lambda_2 - 1} \\ F_{nM}(r_A) &= F_{nM}^{\mathrm{I}}(r_A) + F_{nM}^{\mathrm{II}}(r_A) = W_{nM}^{\mathrm{I}}(r_A) r_A^{\lambda_1 - 1} + W_{nM}^{\mathrm{II}}(r_A) r_A^{\lambda_2 - 1} \\ F_{tI}(r_A) &= F_{tI}^{\mathrm{I}}(r_A) + F_{tI}^{\mathrm{II}}(r_A) = W_{tI}^{\mathrm{I}}(r_A) r_A^{\lambda_1 - 1} + W_{tI}^{\mathrm{II}}(r_A) r_A^{\lambda_2 - 1} \\ F_{nI}(r_A) &= F_{nI}^{\mathrm{I}}(r_A) + F_{nI}^{\mathrm{II}}(r_A) = W_{nI}^{\mathrm{I}}(r_A) r_A^{\lambda_1 - 1} + W_{nI}^{\mathrm{II}}(r_A) r_A^{\lambda_2 - 1} \end{aligned} \tag{3}$$

$$\begin{aligned} & W_{tM}^{\mathrm{I}}(r_A) = \sum_{n=1}^{M} a_n r_A^{n-1}, \quad W_{nM}^{\mathrm{I}}(r_A) = \sum_{n=1}^{M} b_n r_A^{n-1}, \quad W_{tM}^{\mathrm{II}}(r_A) = \sum_{n=1}^{M} c_n r_A^{n-1}, \quad W_{nM}^{\mathrm{II}}(r_A) = \sum_{n=1}^{M} d_n r_A^{n-1} \\ & W_{tI}^{\mathrm{I}}(r_A) = \sum_{n=1}^{M} e_n r_A^{n-1}, \quad W_{nI}^{\mathrm{I}}(r_A) = \sum_{n=1}^{M} f_n r_A^{n-1}, \quad W_{tI}^{\mathrm{II}}(r_A) = \sum_{n=1}^{M} g_n r_A^{n-1}, \quad W_{nI}^{\mathrm{II}}(r_A) = \sum_{n=1}^{M} h_n r_A^{n-1} \end{aligned} \tag{4}$$

In eqn(3), $r_A^{\lambda_1 - 1}$ is a fundamental density to express symmetric type stress singularity, and $r_A^{\lambda_2 - 1}$ is a fundamental density to express skew-symmetric type stress singularity. Here, the eigenvalues λ_1 and λ_2 are given as the roots of the eigenequations.

Figure 2 is an example of the division of the boundary. The weight functions $W_{nM}^{\mathrm{I}} \sim W_{tI}^{\mathrm{II}}$ are chosen as piecewise smooth functions determined at each segment as shown in eqn (4). The body force densities are expressed as shown in eqns(3), (4) in the region of C-A-E in Fig.2. In other region of C-A-E , the boundary condition can be satisfied in a similar way. In this case symmetric and skew-symmetric type of distribution body force are not used.

By using the numerical method mentioned above, the integral equations are reduced to determining the unknown coefficients $a_n \sim h_n$ in eqn (4). They are determined from the boundary conditions at the suitably chosen collocation points at each segment. The stress intensity factors K_{I,λ_1}, $K_{\mathrm{II},\lambda_2}$ for the corner of the cylindrical inclusion can be obtained from the values of $W_n^{\mathrm{I}}(0)$, $W_n^{\mathrm{II}}(0)$, $W_t^{\mathrm{I}}(0)$, $W_t^{\mathrm{II}}(0)$ at the corner tip [4].

3. RESULTS AND DISCUSSION

In Fig.1, extended stress intensity factors K_{I,λ_1} and $K_{\mathrm{II},\lambda_2}$ defined at corner A are analyzed with varying geometrical parameters L / D and elastic ratio G_I / G_M. In the following discussion, dimensionless stress intensity factors F_{I,λ_1} and $F_{\mathrm{II},\lambda_2}$ are shown assuming $\nu_M = \nu_I$ =0.3.

$$F_{\mathrm{I},\lambda_1} = K_{\mathrm{I},\lambda_1} \Big/ \sigma_Z^{\infty} \sqrt{\pi} (D/2)^{1-\lambda_1}, \quad F_{\mathrm{II},\lambda_2} = K_{\mathrm{II},\lambda_2} \Big/ \sigma_Z^{\infty} \sqrt{\pi} (D/2)^{1-\lambda_2} \tag{5}$$

In Tables 1 and 2 F_{I,λ_1} and $F_{\mathrm{II},\lambda_2}$ are shown with increasing the number of collocation points. Theses values, which are determined from the values $W_{\theta,k}^{\mathrm{I}}(0)$, $W_{r,k}^{\mathrm{I}}(0)$, or $W_{\theta,k}^{\mathrm{II}}(0)$, $W_{r,k}^{\mathrm{II}}(0)$, should be in agreement within the error of numerical calculation.

Table 1 Convergence of F_{I,λ_1} and $F_{\mathrm{II},\lambda_2}$ at the corner A ($\nu_I = \nu_M$=0.3, L/D= 10^2, $G_I / G_M = 10^2$)

M	F_{I,λ_1} (λ_1=0.76323491)			$F_{\mathrm{II},\lambda_2}$ (λ_2=0.62184397)		
	from $W_n^{\mathrm{I}}(0)$	from $W_t^{\mathrm{I}}(0)$	Average	from $W_n^{\mathrm{II}}(0)$	from $W_t^{\mathrm{II}}(0)$	Average
2	2.0722	1.9516	2.0119	2.7830	2.7426	2.7628
3	2.1158	2.0741	2.0949	2.8618	2.8586	2.8602
4	2.1305	2.0940	2.1123	2.8804	2.8860	2.8832
5	2.1309	2.0946	2.1128	2.8836	2.8907	2.8872
6	2.1310	2.0946	2.1128	2.8844	2.8946	2.8895

Table 2 Convergence of F_{I,λ_1} and $F_{\mathrm{II},\lambda_2}$ at the corner A ($\nu_I = \nu_M$=0.3, L/D= 10^3, $G_I / G_M = 10^{-2}$)

M	F_{I,λ_1} (λ_1=0.55831618)			$F_{\mathrm{II},\lambda_2}$ (λ_2=0.91168001)		
	from $W_n^{\mathrm{I}}(0)$	from $W_t^{\mathrm{I}}(0)$	Average	from $W_n^{\mathrm{II}}(0)$	from $W_t^{\mathrm{II}}(0)$	Average
2	0.3600	0.3635	0.3618	1.5708	1.6342	1.6025
3	0.3609	0.3638	0.3624	1.6090	1.6384	1.6237
4	0.3628	0.3636	0.3632	1.6124	1.6381	1.6253
5	0.3601	0.3637	0.3619	1.6197	1.6389	1.6293
6	0.3601	0.3637	0.3619	1.6229	1.6393	1.6311

As shown in Tables 1, 2, the errors between these and the average values are within about one percent, and all of them have good convergence. The values obtained from different weight functions of the body forces in n- and t-directions coincided with each other about to the third digit when M= 6 or 8 through the present method.

In Table 3, the results of two rectangular inclusions under longitudinal tension are shown. In Fig.3 F_{I,λ_1} and F_{II,λ_2} vs l_2/d relations are shown. It is found that interaction appears largely at internal point B. At the outside point A, the interaction is not very large. As shown in Fig.4, when two rectangular inclusions are subjected to remote tension in the α direction the results are shown in Fig. 5. In this figure, the interaction appears largely at $\alpha = 90^\circ$ (y-direction) when G_I / G_M >1.

Figure 6 shows F_{I,λ_1} (or F_{II,λ_2}) values for cylindrical inclusion at the corner A with varying parameters L / D and G_I / G_M under longitudinal tension. On the other hand, Fig.7 shows F_{I,λ_1} (or F_{II,λ_2}) values for rectangular inclusion. From those figures, the variations appear in a similar way in 2D and 3D models of fiber. Figure 8 shows the ratios of the results of cylindrical inclusion to the ones of a rectangular inclusion. In this figure, 3D results are usually smaller than 2D results by 10~20 % when G_I / G_M <1. On the other hand, when G_I / G_M >1, 3D results are larger than 2D results by 0~40 %

Table 3 F_{I,λ_1} and F_{II,λ_2} for two rectangular inclusion at the corner A and B under longitudinal tension (Plane strain $\nu_I = \nu_M$=0.3)

Longitudinal tension

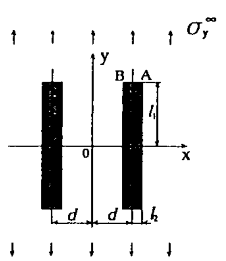

l_1/l_2	l_2/d	G_I/G_M	$F_{I,\lambda_1} = K_{I,\lambda_1}/\sigma^\infty\sqrt{\pi} l_2^{1-\lambda_1}$ 10^{-3}	10^{-2}	10^{-1}	10^{1}	10^{2}	10^{3}	$F_{II,\lambda_2} = K_{II,\lambda_2}/\sigma^\infty\sqrt{\pi} l_2^{1-\lambda_2}$ 10^{-3}	10^{-2}	10^{-1}	10^{1}	10^{2}	10^{3}
10^0	0	AB	0.505	0.476	0.327	0.213	0.224	0.225	2.139	2.159	2.361	±0.493	±0.385	±0.383
	1/3	A	0.525	0.494	0.335	0.204	0.212	0.212	2.139	2.157	2.350	0.503	0.395	0.393
		B	0.555	0.522	0.355	0.211	0.220	0.222	2.124	2.141	2.332	-0.499	-0.390	-0.387
	1/2	A	0.547	0.513	0.343	0.195	0.200	0.200	2.174	2.191	2.371	0.510	0.404	0.403
		B	0.606	0.571	0.388	0.213	0.222	0.224	2.228	2.241	2.407	-0.481	-0.372	-0.368
	2/3	A	0.580	0.543	0.355	0.185	0.189	0.190	2.223	2.244	2.411	0.517	0.411	0.410
		B	0.639	0.602	0.410	0.207	0.212	0.213	2.418	2.427	2.572	-0.421	-0.313	-0.309
10^1	0	AB	0.514	0.489	0.351	0.495	0.673	0.698	1.968	1.979	2.135	±0.944	±1.018	±1.058
	1/3	A	0.583	0.550	0.379	0.466	0.593	0.587	2.017	2.030	2.189	0.856	0.903	1.007
		B	0.517	0.490	0.347	0.416	0.529	0.578	1.999	2.010	2.165	-0.810	-0.754	-0.668
	1/2	A	0.621	0.585	0.398	0.470	0.593	0.591	2.054	2.066	2.216	0.856	0.912	1.000
		B	0.466	0.444	0.323	0.372	0.456	0.503	1.976	1.990	2.147	-0.760	-0.654	-0.554
	2/3	A	0.656	0.617	0.416	0.473	0.593	0.600	2.086	2.096	2.238	0.868	0.931	1.001
		B	0.398	0.382	0.290	0.325	0.386	0.423	1.930	1.942	2.117	-0.711	-0.562	-0.480
10^2	0	AB	0.498	0.483	0.347	0.636	1.543	1.984	1.930	1.930	2.083	±1.224	±2.377	±3.064
	1/3	A	0.605	0.569	0.382	0.683	1.455	1.666	2.003	1.994	2.130	1.208	2.101	2.605
		B	0.375	0.391	0.315	0.537	1.039	1.255	1.823	1.860	2.073	-1.127	-1.679	-1.751
	1/2	A	0.632	0.591	0.398	0.695	1.469	1.678	2.024	2.003	2.145	1.233	2.185	2.697
		B	0.316	0.349	0.296	0.491	0.931	1.138	1.753	1.812	2.050	-1.086	-1.514	-1.506
	2/3	A	0.651	0.614	0.410	0.702	1.456	1.706	2.029	2.004	2.166	1.266	2.267	2.778
		B	0.255	0.304	0.272	0.434	0.802	0.993	1.682	1.771	2.027	-1.033	-1.338	-1.286

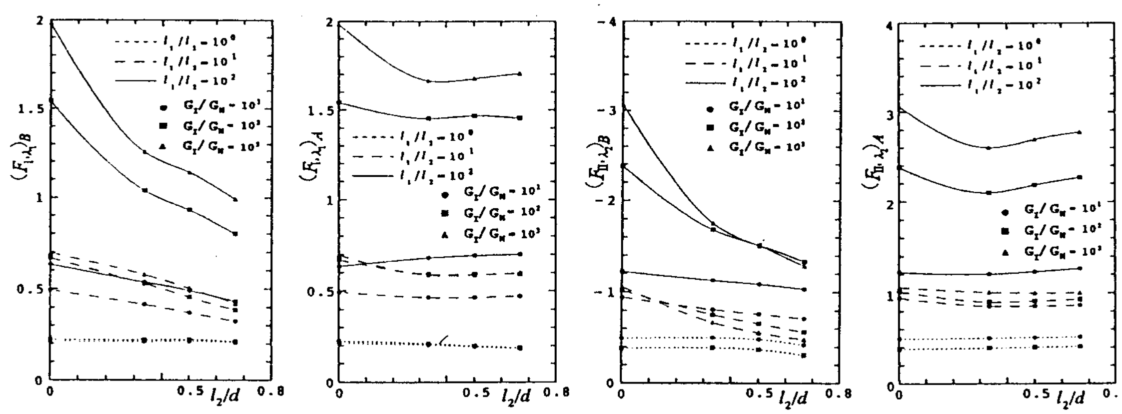

Fig.3 F_{I,λ_1}, F_{II,λ_2} vs l_2/d relations for two rectangular inclusion at the corners A and B ($\sigma_y^\infty = \sigma^\infty$, $\sigma_x^\infty = 0$, $\tau_{xy}^\infty = 0$, Plane strain $\nu_I = \nu_M$=0.3)

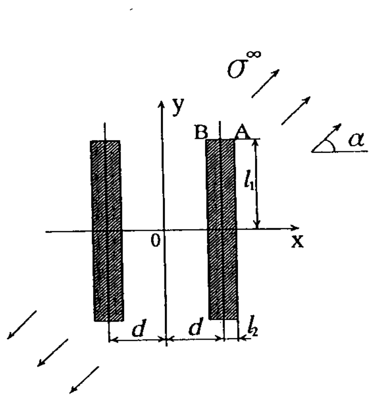

Fig.4 Two rectangular inclusions in a plate Subjected to uniaxial tension in α direction

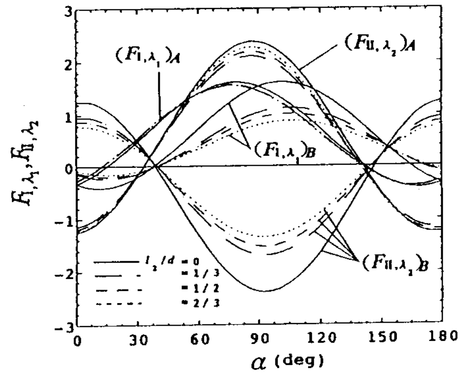

Fig.5 F_{I,λ_1}, F_{II,λ_2} vs α relations at the corners A and B in Fig.3 ($l_1/l_2=10^2$, $G_I/G_M=10^2$, Plane strain $\nu_I=\nu_M=0.3$)

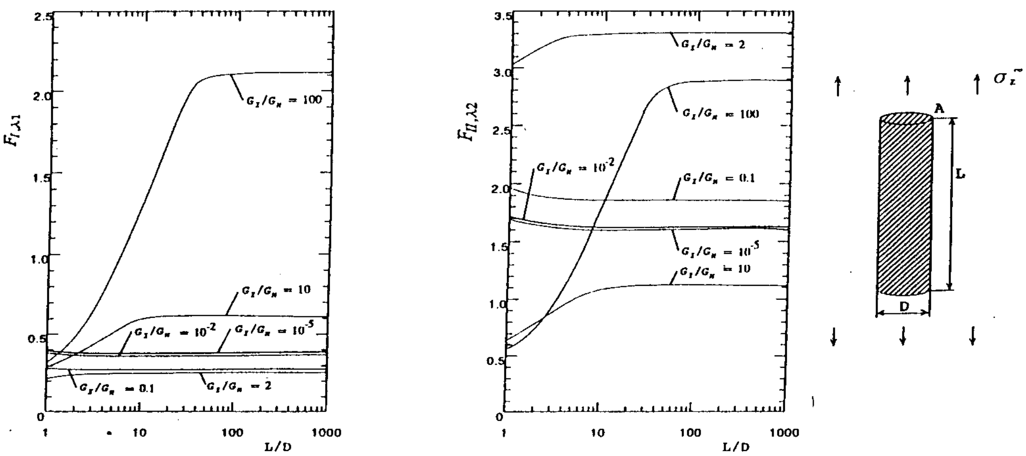

Fig.6 F_{I,λ_1} or $F_{II,\lambda 2}$ at the end of a cylindrical inclusion

4.Conclusions

In this paper, as 3D and 2D models of fibers in composite materials cylindrical and rectangular inclusions were analyzed very accurately, and newly defined stress intensity factors at the fiber end were discussed. The conclusions can be made as follows.

(1) In the numerical solution of the singular integral equations of the body force method, the unknown functions were approximated by the products of fundamental density functions and power series along short segments into which the whole boundary is discretized. It is found that that the present method yields good convergence of the results, and the values of dimensionless stress intensity factors F_{I,λ_1} (or F_{II,λ_2}) obtained from different unknown functions coincide with each other within about 1% when the number of collocation points at each segment is 6 or 8.

(2) When two rectangular inclusions are subjected to remote tension in the α direction as shown in Fig.3, the interaction appears largely at $\alpha=90^\circ$ (y-direction) when $G_I/G_M>1$. The interaction appear largely at the internal point B compared with the outside point A.

(3) The variation of F_{I,λ_1} (or F_{II,λ_2}) values appear in a similar way in 2D and 3D models of fiber with varying aspect ratio L/D. When $G_I/G_M<1$, 3D results are usually smaller than 2D results by 10 ~20%. On the other hand, when $G_I/G_M>1$, 3D results are larger than 2D

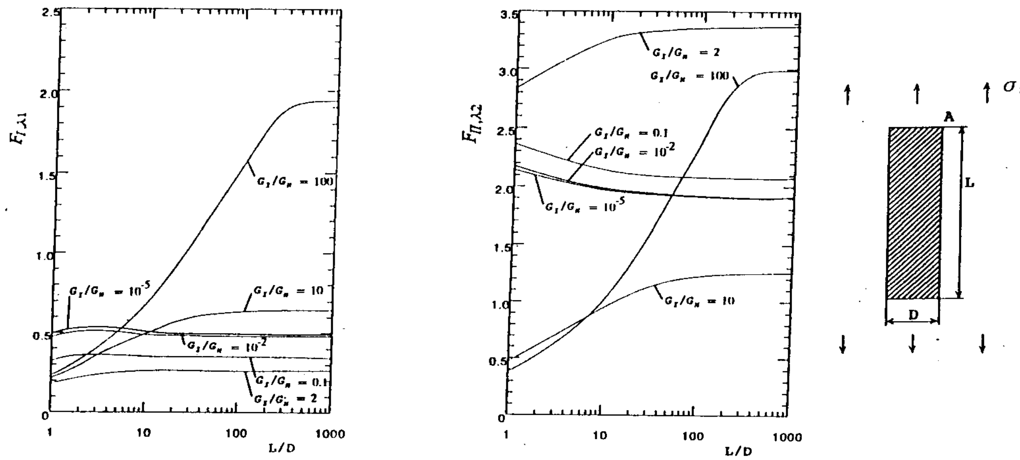

Fig.7 F_{I,λ_1} or F_{II,λ_2} at the end of a rectangular inclusion

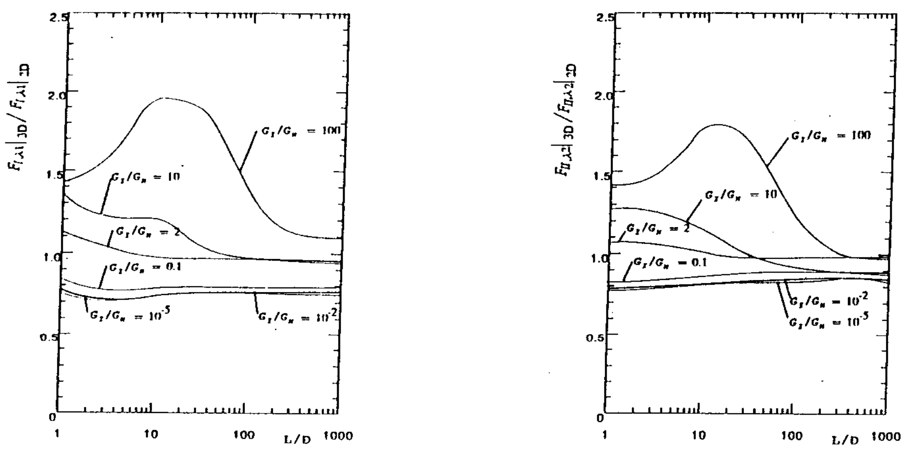

Fig.8 Comparison between cylindrical and rectangular inclusion
($F_{I,\lambda_1\ 3D}/F_{I,\lambda_1\ 2D}$ and $F_{II,\lambda_2\ 3D}/F_{II,\lambda_2\ 2D}$)

results by 0 ~ 40%.

REFERENCE

1. D.H.Chen and H.Nisitani, Singular Stress Field near the Corner of Jointed Dissimilar Materials, Transaction of the ASME, Journal of Applied Mechanics, 1993, 60, 607-613.
2. D.H.Chen and H.Nisitani, Analysis of intensity of singular stress field at fiber end :1st report, Method of analysis , Transaction of the JSME, 1992, 58-554 A, 1834-1838.
3. D.H.Chen and H.Nisitani, Analysis of intensity of singular stress field at fiber end :2nd report, Results and discussion , Transaction of the JSME, 1992, 58-554 A, 1839-1845.
4. N.A.Noda, K.Oda, and Y.Kawashima, Interaction of Newly Defined Stress Intensity Factors for Angular Corners in Two Diamond-Shaped Inclusions, Localized Damage IV, 1996, 709-717.